Multi-parametric liver tissue characterization using MR Fingerprinting: simultaneous T_1, T_2, T_2* and fat fraction mapping

Olivier Jaubert[1], Cristobal Arrieta[2], Gastão Cruz[1], Aurélien Bustin[1], Torben Schneider[3], Georgios Georgiopoulos[1], Pier-Giorgio Masci[1], Carlos Sing-Long[2,4], Rene M. Botnar[1,5], Claudia Prieto[1,5]

[1] School of Biomedical Engineering and Imaging Sciences, King's College London, United Kingdom

[2]Biomedical Imaging Center and Millennium Nucleus for Cardiovascular Magnetic Resonance, Pontificia Universidad Católica de Chile, Chile

[3] Philips Healthcare, Guilford, United Kingdom

[4]Instituto de Ingeniería Matemática y Computacional and Millennium Nucleus for the Discovery of Structures in Complex Data, Pontificia Universidad Católica de Chile, Chile

[5]Escuela de Ingeniería, Pontificia Universidad Católica de Chile, Chile

Short Title: Liver MR Fingerprinting: T_1, T_2, T_2* and fat fraction

Submitted as Note to Magnetic Resonance in Medicine

Main document word count: 3047

Corresponding author:

Name	Olivier Jaubert
Department	School of Biomedical Engineering and Imaging Sciences
Institute	King's College London
Address	3rd Floor, Lambeth Wing, St Thomas' Hospital London SE1 7EH, United Kingdom
E-mail	olivier.jaubert@kcl.ac.uk

Abstract

Purpose: Quantitative T_1, T_2, T_2* and fat fraction (FF) maps are promising imaging biomarkers for the assessment of liver disease, however these are usually acquired in sequential scans. Here we propose an extended Magnetic Resonance Fingerprinting (MRF) framework enabling simultaneous liver T_1, T_2, T_2* and FF mapping from a single ~14s breath-hold scan.

Methods: A gradient echo (GRE) liver MRF sequence with nine readouts per TR, low flip angles (5-15^o), varying magnetisation preparation and golden angle radial trajectory is acquired at 1.5T to encode T_1, T_2, T_2* and FF simultaneously. The 9-echo time-series are reconstructed using a low-rank tensor constrained reconstruction and used to fit T_2*, B_0 and to separate the water and fat signals. Water and fat specific T_1, T_2 and M_0 are obtained through dictionary matching, whereas FF estimation is extracted from the M_0 maps. The framework was evaluated in a standardized T_1/T_2 phantom, a water-fat phantom and 12 subjects in comparison to reference methods. Preliminary clinical feasibility is shown in 4 patients.

Results: The proposed water T_1, water T_2, T_2* and FF maps in phantoms showed high coefficients of determination (r^2>0.97) relative to reference methods. Measured liver MRF values in vivo (mean ±standard deviation) for T_1, T_2, T_2* and FF were 671±60ms, 43.2±6.8ms, 29±6.6ms and 3.2±2.6% with biases of 92ms, -7.1ms, -1.4ms and 0.63% when compared to conventional methods.

Conclusion: A 9-echo liver MRF sequence allows for quantitative multi-parametric liver tissue characterization in a single breath-hold scan of ~14s. Future work will aim to validate the proposed approach in patients with liver disease.

Keywords: MR Fingerprinting, Liver MRI, T1 mapping, T2 mapping, T2* mapping, Fat Fraction, Quantitative mapping

Introduction

Non-alcoholic fatty liver disease (NAFLD) is highly prevalent worldwide (25%) and is associated with many hepatic and extra-hepatic diseases creating an increasingly large clinical and economic burden (1). In the Western and industrialised countries, NAFLD is one of the main causes of cirrhosis and highly prevalent in patients with hepatocellular carcinoma the main causes of liver related deaths (2). Pathogenesis of NAFLD can be subdivided into four stages, which are progressively characterized by fat accumulation, inflammation (non-alcoholic steatohepatitis, or NASH) and potentially leading to irreversible fibrosis (cirrhosis), hepatocellular carcinoma or other life-threatening complications (2). Liver biopsy remains the current reference standard for diagnosing and staging NAFLD; however, they are invasive, costly and potentially hazardous. Liver biopsies are also prone to sampling errors and suffer from inter-rater variability (with agreement of diagnostic category reported at 0.61 (3)).

Quantitative magnetic resonance imaging (MRI) parametric mapping is rapidly emerging as a non-invasive approach for the assessment of fatty liver disease. Quantitative MRI has been applied successfully to map spatially hepatic lipid content using proton density fat fraction (PDFF) (4,5), hepatic iron content using T_2* (6) and to detect fibrosis and inflammation using T_1, T_2 (7) and elastography (8). Multi-parametric quantitative MRI has shown to provide valuable diagnostic and prognostic information by jointly monitoring the different pathophysiologies of the disease (9,10). These multiple scans are usually performed sequentially during separate breath-holds (9), thus leading to long scan times, patient fatigue and potentially mis-registered parameter maps. Joint parameter mapping has been proposed to map liver T_2* and PDFF simultaneously (11) and more recently to map liver T_1, T_2 and M_0 (12), with both methods accounting for inter-parametric dependencies. The first method fits multiple echo images to a multi-peak water-fat signal model with T_2* decay (13,14) while the latter uses Magnetic Resonance Fingerprinting (MRF) (15) to generate multiple parametric maps from a highly undersampled acquisition with dynamically varying contrasts. Recent works combining water-fat imaging and MRF have been proposed to map water specific T_1 and T_2 and fat fraction (FF) (16,17) simultaneously to further reduce inter-parametric biases and overall scan time.

Here we propose to jointly map T_1, T_2, T_2* and FF for comprehensive liver tissue characterization. This is achieved by extending our previous work on 3-echo Dixon cardiac

MRF (17) to a 9-echo Gradient Rewound Echo (GRE) acquisition and graphcut method (18) for estimation of B_0 and T_2* and water-fat separation. To the best of our knowledge this is the first time that liver T_1, T_2, T_2* and FF are simultaneously quantified in a single acquisition. The proposed framework was evaluated in phantoms against spin echo T_1 and T_2 and 12-echo GRE (PDFF and T_2*) reference measurements, and in 12 subjects against MOLLI, T2-GRASE and 12-echo GRE. Preliminary clinical feasibility is shown in 4 patients.

Methods

The proposed framework combines 1) a 9-echo GRE acquisition; 2) a B_0 and B_1 insensitive acquisition scheme using fixed repetition time (TR), gradient spoiling, low flip angles (FA) and magnetization preparations; 3) an undersampled reconstruction with temporal compression and patch-based low-rank tensor regularization; 4) a graphcut based method for estimation of B_0, T_2* and water-fat fractions; 5) a dot-product matching step and 6) a FF estimation step from the relative proton density (M_0) images. Details of the framework are described below.

Acquisition

The proposed liver MRF acquisition (Figure 1) consists of a 9-echo, golden angle radial (~111°) GRE acquisition with bipolar readouts and varying inversion (IR) and T_2 preparation (T2prep) pulses (17). The acquisition scheme includes T2 preps with four adiabatic refocusing pulses (19) and varying durations, noted as T2prepX, and hyperbolic hypersecant IR pulses with varying inversion delays, noted as TIY, where X and Y are durations in ms. A total of 12 magnetization preparations followed by data acquisition are applied during a single breath-hold scan of 13.9s with the following pattern: TI12, no preparation (noPrep), T2prep40, T2prep80, T2prep160, TI300, noPrep, T2prep40, T2prep80, T2prep160, TI12, noPrep. The data acquisition block consists of varying low FAs (9 linear ramp-up RF pulses from 5^o to 15^o followed by 26 fixed 15^o RF pulses (20)), 35 TRs, bandwidth 746 Hz/pixel, 9 echoes per TR, TR/TE1/ΔTE= 20/1.5/2ms leading to 700ms data acquisition blocks. Acquisition blocks are spaced regularly every 1.2s allowing for recovery (varying between ~200-500ms) before the next magnetization preparation module. A fixed TR, low FAs and 4π gradient spoiling along slice selection were used to reduce the sensitivity to B_0 and B_1 inhomogeneities (20–22).

Image Reconstruction

MRF time-series reconstruction was performed using a multi-contrast patch-based high-order low-rank reconstruction (HD-PROST) (23) with temporal dictionary based compression. Temporally compressed singular images $\mathbf{x}_\mathrm{i} = {\mathbf{U}_\mathrm{R}}^\mathrm{H}\mathbf{x}'_\mathrm{i}$ approximating the MRF time-series $\mathbf{x}'_\mathrm{i}$ (24,25) are reconstructed for each echo i using HD-PROST, where $\mathbf{U}_\mathrm{R}$ are the left singular vectors of the MRF dictionary matrix truncated to rank R. Reconstruction parameters included a rank R=6 and a sparsity promoting parameter $\lambda = 10^{-3}$ (17,23).

T_2, B_0 and water-fat separation*

Given a water ($\mathbf{W}'$) and a set of fat ($\mathbf{F_k}'$) compartments time-series (14,26,27), the reconstructed singular images at echo i, can be written as :

$$\begin{aligned}\mathbf{x}_\mathrm{i} = {\mathbf{U}_\mathrm{R}}^\mathrm{H}\mathbf{x}'_\mathrm{i} &= {\mathbf{U}_\mathrm{R}}^\mathrm{H}\left(\mathbf{W}' + \sum_l \mathbf{F}_l'\ e^{j2\pi\Delta f_l t_i}\right)e^{-\frac{t_i}{T2^*}+j2\pi\Delta f_{B0}t_i} \\ &= (\mathbf{W}+\mathbf{F})e^{-\frac{t_i}{T2^*}+j2\pi\Delta f_{B0}t_i}\end{aligned} \quad [3]$$

Where $\mathbf{W}$ and $\mathbf{F} = {\mathbf{U}_\mathrm{R}}^\mathrm{H}\sum_l \mathbf{F}_l'\, e^{j2\pi\Delta f_l t_i}$ are the water and fat (or combined fat compartments) singular images, Δf_l is the known difference in precession frequency between water and fat compartment l, Δf_{B0} is the precession frequency difference induced by B_0 field inhomogeneities and t_i is the echo time i. A graph-cut scheme (18) is used to solve for B_0, T_2* and water-fat separation using a pre-defined 6-peak fat model (28). First singular images of all echo times are used for B_0 and T_2* estimation. The resulting maps are subsequently used to separate the other singular images by pseudo inverse (29) into water and fat. This model ignores the different T_1 and T_2 values (28) of the fat peaks which can lead to varying signal peak weights during the MRF acquisition. The impact of this simplified model was investigated in simulations.

T_1, T_2 and fat fraction maps

The water and fat singular images are then matched (using dot-product) to a previously generated MRF dictionary (with fixed TE=0^+ ms) to obtain the water and fat specific T_1, T_2 and relative M_0 maps. The dictionary was generated using the extended phase graph formalism (30) including slice profile (31) (51 points along the slice profile) and inversion efficiency (20) corrections. The dictionary contained signal evolutions corresponding to combinations of T_1

and T_2 of interest (i.e. [50:10:1400, 1430:30:1600, 1700:100:2200, 2400:200:3000] ms for T_1 and [5:2:80, 85:5:150, 160:10:300, 330:30:600] ms for T_2 as well as the standardized T_1/T_2 phantom (32) reference values. The FF map is estimated from the water and fat M_0 and phase images (for noise bias correction (17,33)).

Experiments

Experiments were performed on phantoms and 2 cohorts of subjects. Cohort 1 (12 subjects, 7 females, age: 31 ± 4 years, body mass index (BMI): 23.9 ± 3.5 kg/m^2) underwent the proposed liver MRF and conventional techniques. Cohort 2 (4 subjects, 1 female, age: 56 ± 13 years, BMI: 27.9± 4.0 kg/m^2) underwent only the proposed liver MRF during a clinically referred scan. Cohort 2 had large BMI >25 kg/m^2 or previously diagnosed liver iron overload. All experiments were approved by the Institutional Review Board and written informed consent was given by all participants before scanning. Acquisitions were performed on a 1.5T Ingenia MR scanner (Philips Healthcare, The Netherlands).

Preliminary experiments investigated the number of echoes necessary for T_2* mapping in phantom (Supporting Information Text S1) and the performance of the framework in numerical simulations (Supporting Information Text S2 and Figure S1).

Phantom study

Acquisitions were performed on a standardized T_1/T_2 phantom (T1MES) with 0% fat (32) and on a water-fat phantom built in-house. The standardized T_1/T_2 phantom was used to validate the water T_1 and T_2 measurements against T_1 inversion recovery spin echo (IRSE) and T_2 multi-echo spin echo (MESE). The reference T_1 and T_2 methods do not consider fat suppression/separation thus only the phantom with 0% fat was employed to validate the T_1 and T_2 measurements avoiding biases due to incomplete fat suppression. FF and T_2* measurements were performed in the standardized phantom and water-fat phantom and validated against a reference 12-echo GRE. The reference PDFF and T_2* maps were obtained using the same graph cut method (18), fat model and noise bias correction (33) as described for the proposed 9-echo liver MRF. Acquisition and mapping parameters for all reference sequences are included in Supporting Information Table S1.

Scan parameters for the proposed liver MRF were described in the Acquisition section, remaining parameters were: FOV = 496x496mm^2, 2x2mm^2 resolution, 8 mm slice thickness.

In vivo study

The proposed liver MRF T_1, T_2, T_2* and FF maps were validated against reference T_1 MOLLI (5(3)3), T2-GRASE and 12-echo GRE (T_2* and PDFF) respectively in cohort 1. Acquisition parameters for all conventional sequences are included in Supporting Information Table S1. All acquisitions were performed in transversal orientation under breath-hold at end-expiration.

The same liver MRF acquisition was performed on cohort 2 to show preliminary feasibility of the approach in a clinical setting.

Analysis

Regions of interest (ROIs) were manually drawn in each vial of the phantoms. Coefficients of determination, lines of best fit and biases are reported for each parameter map in comparison to their corresponding reference measurements.

For each subject CX.Y (cohort X, subject number Y), ROIs were manually drawn in the liver (in 4 different areas of the liver avoiding blood vessels, the median value is reported), posterior muscle, subcutaneous fat and the spleen. Mean measurements and range in 11 subjects with no history of liver disease (C1.1-10) or benign hemangioma (C1.11) are reported for all parameters for the proposed liver MRF and the corresponding conventional maps. C1.12 has been previously diagnosed with mild liver steatosis. Mean values, range, mean bias, 95% (±1.96 standard deviation) confidence intervals (CI) and coefficients of determination are used to compare the measurement methods for cohort 1. A paired t-test was performed to test for statistically significant differences ($P<0.05$) between the proposed liver MRF and conventional measurements.

Results

Preliminary studies

T_2* maps of the preliminary phantom acquisition (standardized T_1/T_2 and water/fat phantoms) obtained using the first 3, 6, 9 or 12 echoes for map estimation are shown in Supporting Information Figure S2.A. Bland Altmann plots (Supporting Information Figure S2.B) and maps show large bias of T_2* estimation when using only the first 3 echoes, and small bias but noisy measurements when using 6 echoes. Maps obtained using the first 9 echoes compare qualitatively and quantitatively well with the ones obtained using all 12 echoes, albeit enabling

shorter TR and thus scan time. The T_2* map obtained using the first 9 echoes of the 12-echo MRF acquisition presented a mean bias of 1.4 ms when compared to the reference T_2* map obtained from a conventional 12-echo GRE scan.

Numerical simulations of the proposed framework led to accurate (<1%) liver T_2* and B_0 estimation and ensuing water T_1, water T_2 and FF estimation despite the simplified model used for water-fat separation (Supporting Information Figure S3), although overestimation of subcutaneous fat T_2* was observed. Simulated errors in the estimation of B_0 before water-fat separation caused significant errors in FF maps (>9%) and low errors in water T_1 or T_2 maps (<20ms and <1ms respectively) (Supporting Information Figure S4 and S5). Errors in T_2* did not show an effect in the subsequent T_1, T_2 and FF estimation.

Phantom study

Water T_1, water T_2, FF and T_2* maps for the proposed MRF approach (Supporting Information Figure S6) are quantitatively compared to T_1 IRSE, T_2 MESE and T_2* and FF (12-echo GRE) reference maps (Figure 2.A). Correlation plots with lines of best fit show high coefficients of determination for water T_1 and water T_2 (standardized phantom only, 0% fat) (r^2>0.99) and for FF and T_2* (standardized and water-fat phantoms) (r^2>0.97). Biases were measured at -15ms, -4.7ms, 1.9ms and -0.5% for T_1, T_2, T_2* and FF respectively. The bias for short T_2s (0.73 ms) was smaller than for T_2s outside the range of interest (T_2 >80ms).

In vivo study

Water T_1, water T_2, FF and T_2* ROI measurements for the proposed liver MRF in subjects C1.1-12 are compared to conventional techniques (Figure 2.B) showing high coefficients of determination (r^2>0.93) for all parameters. Water T_1 and T_2 measurements were not performed in the subcutaneous fat ROI due to its low water content.

Liver values (mean [min, max]) measured in subjects C1.1-11 with the proposed approach were 676ms [607, 803]ms for water T_1, 43.6ms [35.9, 57.8]ms for water T_2, 30.1ms [17.9, 39]ms for T_2* and 2.56% [1.2, 5.3]% for FF. Corresponding mean values and range for muscle, spleen and subcutaneous fat are reported in Supporting Information Table S2 in comparison to the conventional methods and literature values (34–36) when available. Fat specific T_1 and T_2 are reported for the subcutaneous fat ROI. Boxplots showing T_1, T_2, FF and T_2* mean, median, interquartile, standard deviation and outliers obtained with the proposed liver MRF and

conventional sequences are included in Figure 3 for subjects C1.1-12. Biases and CI (bias [CI]) observed with the proposed liver MRF in comparison to conventional methods for all ROIs combined (excluding subcutaneous fat for water T_1 and T_2 measurements due to its low water content) were 110ms [23;200]ms for water T_1, -9.1ms [-18;-0.19]ms for water T_2, 2.1ms [-8.6;13]ms for T_2* and 0.32% [-4.4;5.0]% for FF. For liver measurements alone slightly lower biases and tighter CI were observed (i.e. 92ms [18;170]ms, -7.1ms [-12;-2.2]ms, -1.4ms [-4.4;1.5]ms and 0.63% [-1.4;2.7]% for T_1, T_2, T_2* and FF respectively) with statistically significant differences for T_1, T_2 and T_2*.

Water T_1, water T_2, FF, T_2* and B_0 maps for the proposed liver MRF are shown for two subjects in comparison to the corresponding conventional mapping techniques (Figure 4). An elevated liver FF was measured in subject C1.12 at 10.3% with the proposed approach and 9.2% with conventional PDFF (Figure 4.A). Subject C1.11, with a previously diagnosed benign hemangioma (i.e. abnormal mass of small blood vessels), is shown in Figure 4.B. Water T_1, water T_2, T_2* and FF in the hemangioma were measured at 1603 ms, 112 ms, 80 ms and 1.2% with the proposed liver MRF and 1469 ms, 163 ms, 71ms and -0.2% with conventional methods respectively.

Water T_1, water T_2, FF, T_2* and B_0 maps for the proposed liver MRF are shown in Figure 5 for all cohort 2. C2.2-4 presented elevated liver FF (15.25%, 12.45% and 18%, respectively) with water T_1, water T_2 and T_2* values within the range obtained in cohort 1.1-11 (Supporting Information Table S2) for C2.2 and C2.3 and abnormally low for C2.4 (520ms, 20.9ms, 1.95ms, respectively) consistent with previously diagnosed elevated hepatic iron concentration.

Discussion

A 9-echo MRF approach is proposed for multi-parametric and simultaneous T_1, T_2, T_2* and fat fraction (FF) liver tissue characterization in a single 14s acquisition. The proposed approach relies on the reconstruction of a transient signal sampled for different echo times. The echo sampling allows for T_2* and B_0 estimation and separation of the transient signal into a water and fat fingerprints. The fingerprints can then be used for MRF dictionary matching to obtain water and fat T_1, T_2 and relative M_0 maps, whereas FF can be estimated from the water and fat M_0 maps. Compared to previous water-fat MRF works using multi-peak fat models (16,17,37), in this work T_2* decay is included in the signal model (Eq.3) to improve water and fat separation and additionally map T_2* for liver iron content assessment. Dictionary based

methods (37,38) could be investigated for single step FF, water and fat T_1 and T_2, T_2* and B_0 estimation however this may lead to challenging dictionary sizes while relying on single voxel information. Chemical shift based approaches (18,39) usually enforce B_0 field smoothness for robust estimation and water-fat separation. Previously proposed water-fat MRF works have used these approaches (16,40,41) but mapped less parameters and required an additional (separately acquired) B_1 map.

Phantom experiments show high coefficients of determination between the proposed approach and reference measurements for the T_1, T_2, T_2* and FF ranges of interest. Good agreement of the B_0 maps (Figure 4) and low FF errors compared to those observed in simulations suggest accurate B_0 estimation. Sequence modifications might be necessary if the tissue of interest has long T_2 and T_2*. Biases with respect to conventional and literature values were observed in vivo. These are expected for a few reasons: 1) Magnetization transfer effects in biological tissues and flow are expected to bias MRF (42–44) as well as conventional (45) measurements. 2) In vivo conventional mapping present their own biases and are suboptimal references (e.g. MOLLI has a tendency to underestimate T_1 (46,47) and T2-GRASE to overestimate T_2 when compared to T2-prep bSSFP (48)). Moreover, previously proposed MRF approaches (17,20,49) have shown overestimation of T_1 when compared to MOLLI and underestimation of T_2 compared to conventional scans in vivo. 3) Acquisitions were performed sequentially during separate breath-holds leading to potentially mis-registered MRF and conventional measurements. 4) Fat model simplifications led to overestimation of T_2* in subcutaneous fat in simulations and in vivo. Despite these biases, good correlations were obtained in vivo between the proposed approach and conventional techniques. The proposed approach requires shorter scan time and fewer breath-holds while keeping similar resolutions as those proposed in recent multi-parametric (50) and NAFLD clinical studies (51–53). Additionally, it provides inherently co-registered maps ensuring mapping of the same slice of the liver for all parameters and enabling pixel-wise multi-parametric measurements.

Water-fat separation and T_2* corrections do not correct for the effect of iron content on T_1 and T_2 measurements directly as seen in subject C2.4 (Figure 5) however additional corrections could be incorporated to better correlate results with biopsy fibrosis scores in the presence of iron overload (54). This would require simulating multiple compartments and magnetization transfer effects (44) while making strong model assumptions (54). Further investigation of the precision (reproducibility) and accuracy of this framework in clinical settings is still needed.

Conclusion

A multi-echo MRF framework is proposed for fast and simultaneous quantitative multi-parametric liver tissue characterization. Co-registered parametric maps (water T_1, water T_2, T_2* and FF) are acquired in a single breath-hold (13.9s). The proposed approach was validated in phantoms showing good correlation with reference measurements. The feasibility of the proposed approach was evaluated in vivo in 16 subjects. Future investigation in patients with liver disease is now warranted.

Acknowledgments

This work was supported by the following grants: (1) EPSRC EP/P032311/1, EP/P001009/1 and EP/P007619/1, (2) BHF programme grant RG/20/1/34802, (3) King's BHF Centre for Research Excellence RE/18/2/34213 (4) Wellcome EPSRC Centre for Medical Engineering (NS/A000049/1), and (5) the Department of Health via the National Institute for Health Research (NIHR) Cardiovascular Health Technology Cooperative (HTC) and comprehensive Biomedical Research Centre awarded to Guy's & St Thomas' NHS Foundation Trust in partnership with King's College London and King's College Hospital NHS Foundation Trust. CA and CSL received funding from Millennium Science Initiative of the Ministry of Economy, Development and Tourism, Government of Chile, grant Nucleus for Cardiovascular Magnetic Resonance, and CONICYT PCI-REDES180090. CSL was partially funded by grant Millennium Nucleus Center for Discovery of Structures in Complex Data and CONICYT Fondecyt #11160728. CA was partially funded by CONICYT Fondecyt Postdoctorado 2019 #3190763. GG has been supported by a research fellowship from the European Association of Cardiovascular Imaging. We acknowledge the use of the Fat-Water Toolbox (http://ismrm.org/workshops/FatWater12/data.htm) for some of the results shown in this article.

Figures

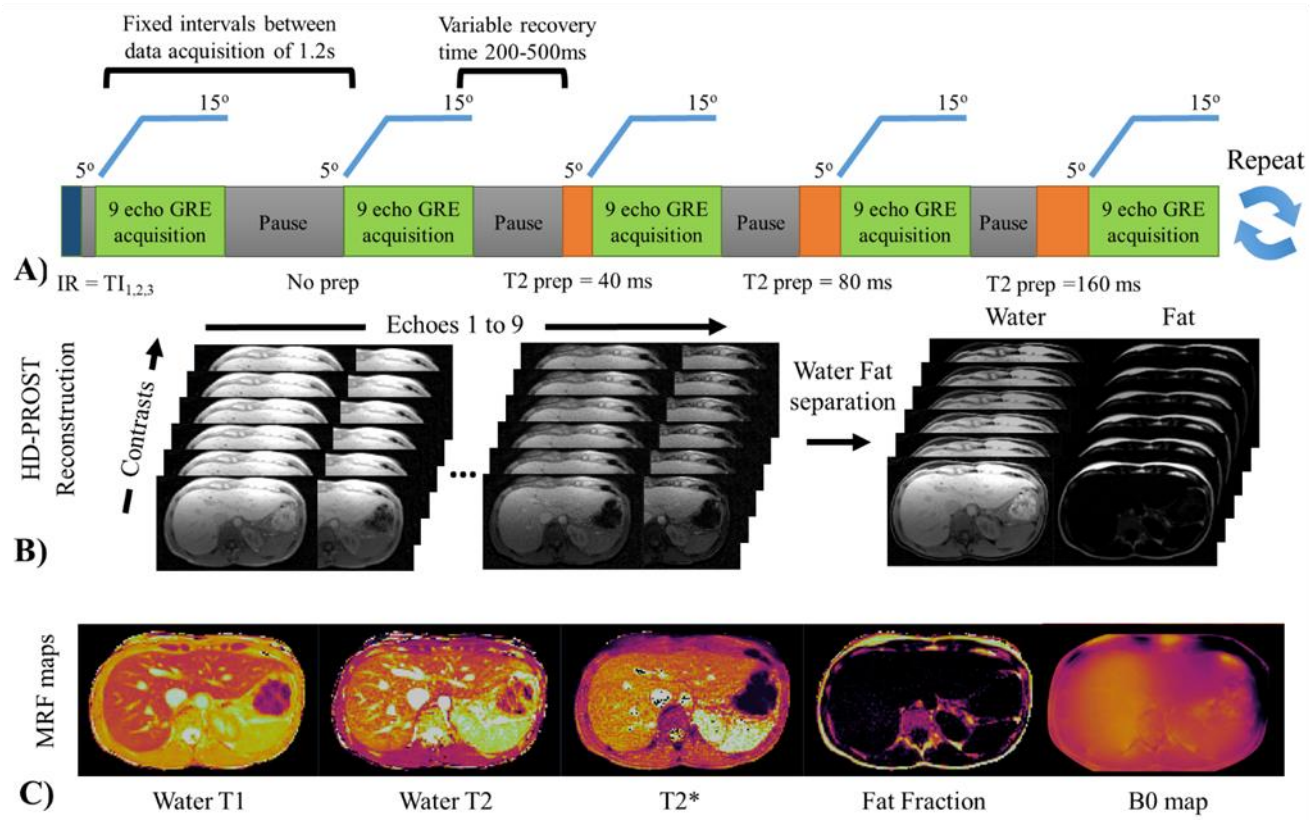

Figure 1. A) The proposed 9-echo liver MRF acquisition consists of 12 acquisition modules (700ms) (5 shown here) with different inversion recovery (IR) and T_2 preparation pulses (and recovery times ~200-500ms) performed in a single ~14s breath-hold scan. B) Images are reconstructed using dictionary-based temporal compression and low-rank patch-based regularization (HD-PROST). The signal from the nine echoes is separated into water and fat components. C) B_0 and T_2* maps are estimated during the separation of the signals. Water and fat specific T_1, T_2 and M_0 maps are obtained through dot product matching to a previously generated MRF dictionary whereas fat fraction is estimated from the water and fat M_0 maps.

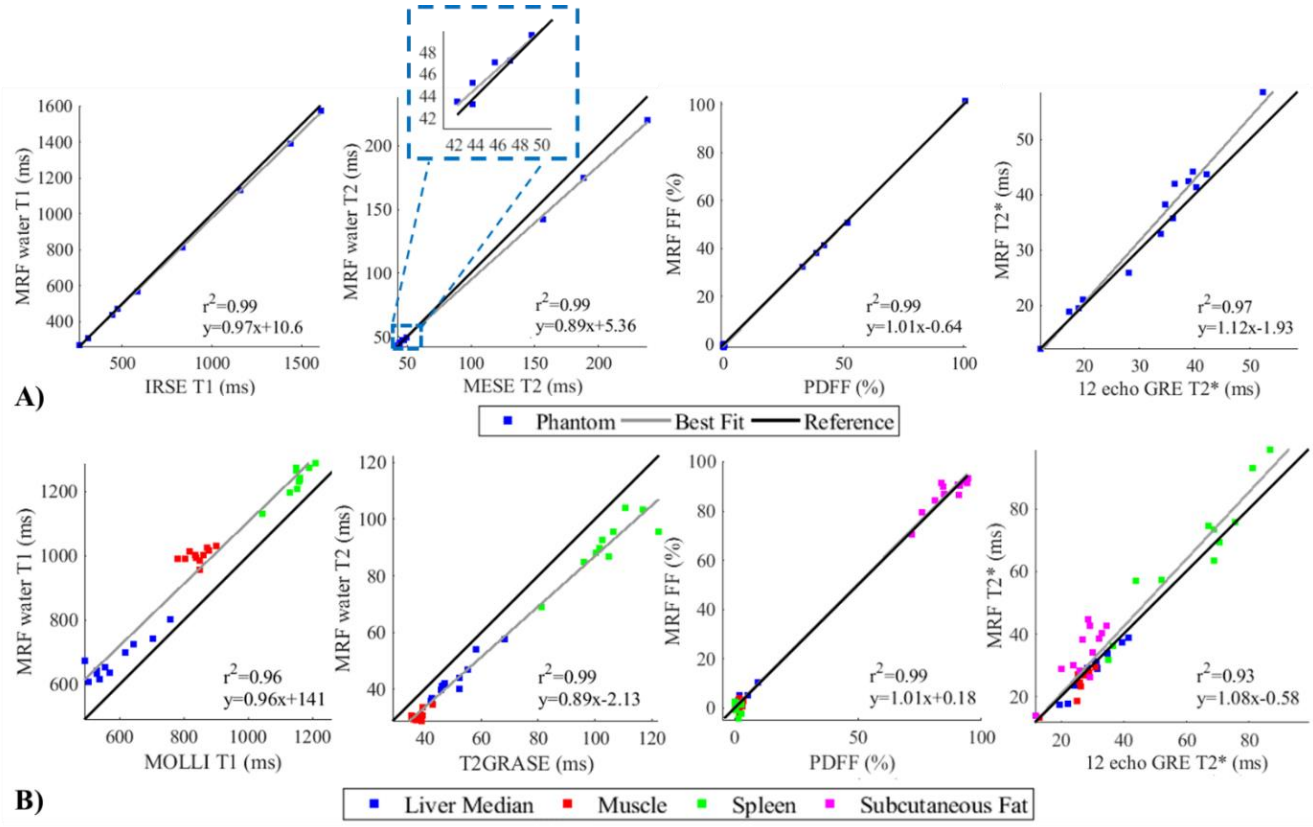

Figure 2. A) Phantom correlation plots comparing water T_1 and water T_2 (standardized T_1/T_2 phantom, 0% fat) and FF and T_2* (standardized T_1/T_2 and water-fat phantoms) measurements obtained from the proposed 9-echo liver MRF and from reference IRSE (T_1), MESE (T_2) and 12-echo GRE (FF/T2*) scans. B) In vivo correlation plots comparing the proposed 9-echo liver MRF approach to conventional MOLLI (T_1), T2GRASE (T_2), and 12-echo GRE (T_2*/FF) scans. Liver (median over 4 ROIs), anterior muscle, spleen and subcutaneous fat (for T_2* and FF estimation only due to its low water content) measurements were performed in cohort 1 (12 subjects).

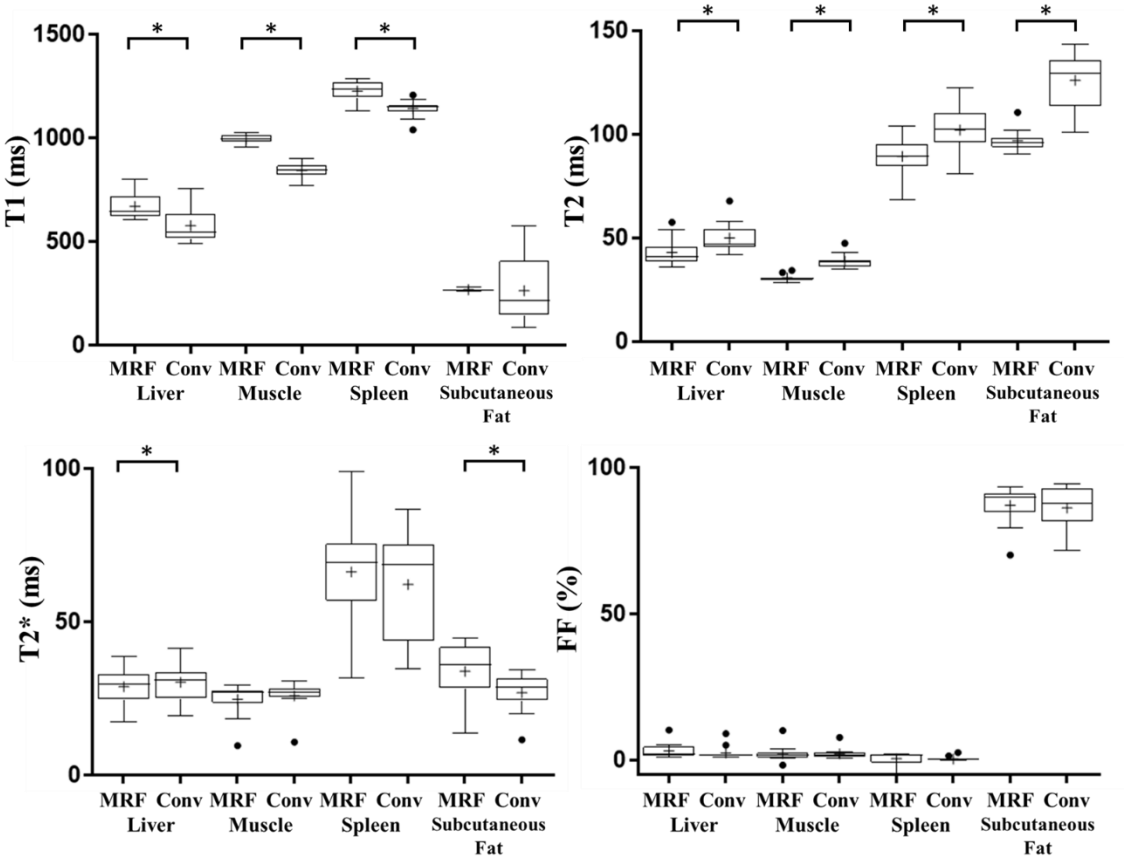

Figure 3. Boxplots showing T_1, T_2, T_2* and FF measurements mean (+), median (__), interquartile range (IQR) (box), Tukey whiskers and remaining outliers (•) obtained in cohort 1 (12 subjects, C1.1-12) for liver, muscle, spleen and subcutaneous fat for proposed 9-echo liver MRF and conventional (Conv) methods (i.e. MOLLI, T2-GRASE, and 12-echo GRE T_2* and PDFF). Statistically significant differences (paired t-test) in mean measurements are indicated with * ($P<0.05$) and are shown for each body organ. Please note that water T_1 and water T_2 are reported for the liver, muscle and spleen ROIs with the proposed MRF approach, whereas fat T_1 and fat T_2 are reported for subcutaneous fat. Numerical mean and full range values for C1.1-11 (with no history of liver disease) are reported in Supporting Information Table S2.

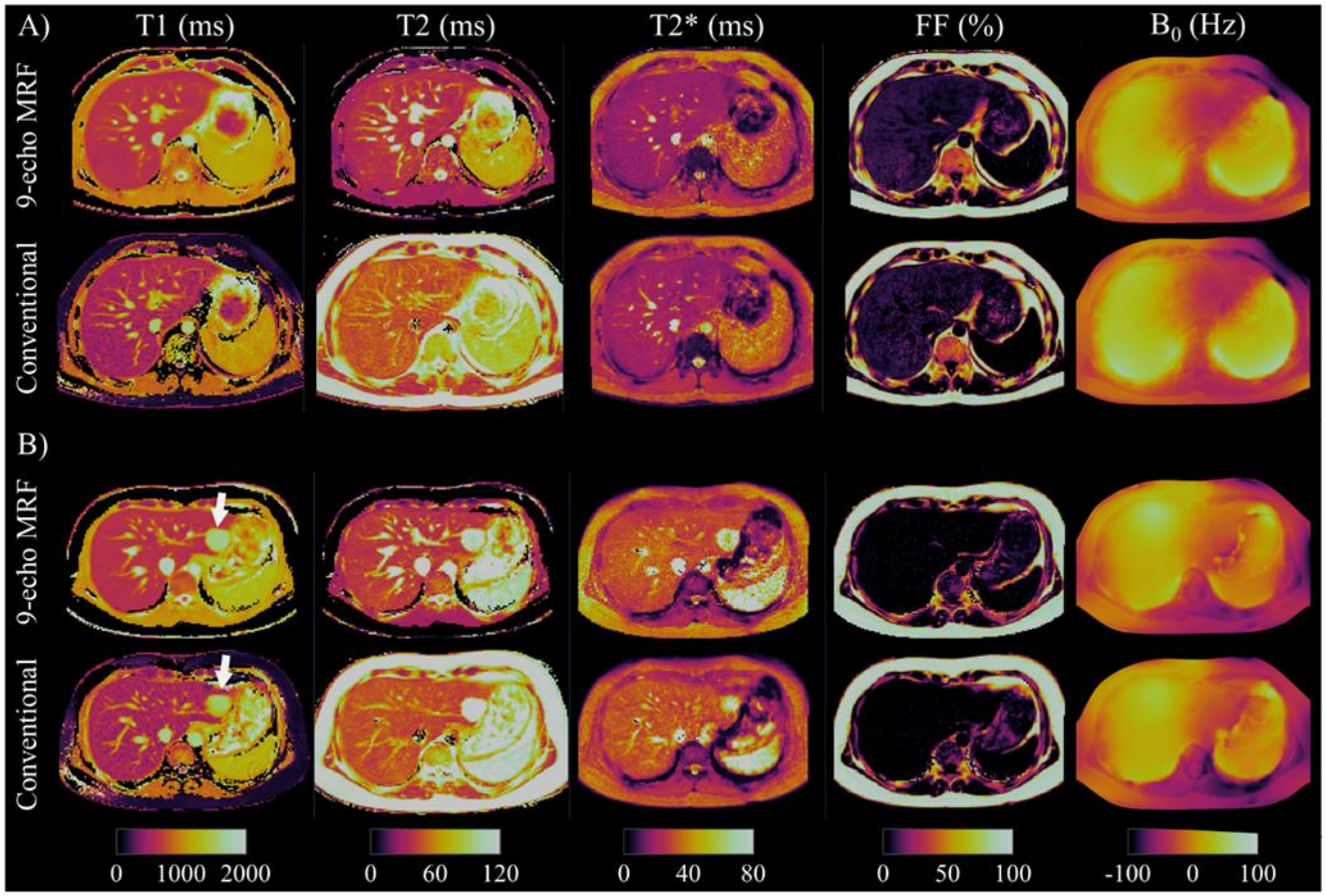

Figure 4. Proposed 9-echo liver MRF water T_1, water T_2, T_2*, FF and B_0 compared to T_1 (MOLLI), T_2 (T_2GRASE), T_2*, PDFF and B_0 (12-echo GRE) maps acquired in three separate breath-holds for two subjects. A) Subject C1.12 presented slightly elevated hepatic fat content, measured at 10.3% with the proposed liver MRF and 9.2% with the conventional method. B) Subject C1.11 presented a previously diagnosed hemangioma, which is visualized in the parametric maps (white arrow on T_1 maps). Water T_1, water T_2, T_2* and FF in the hemangioma were measured at 1603 ms, 112 ms, 80 ms and 1.2% with the proposed liver MRF and 1469 ms, 163 ms, 71ms and -0.2% with the corresponding conventional methods.

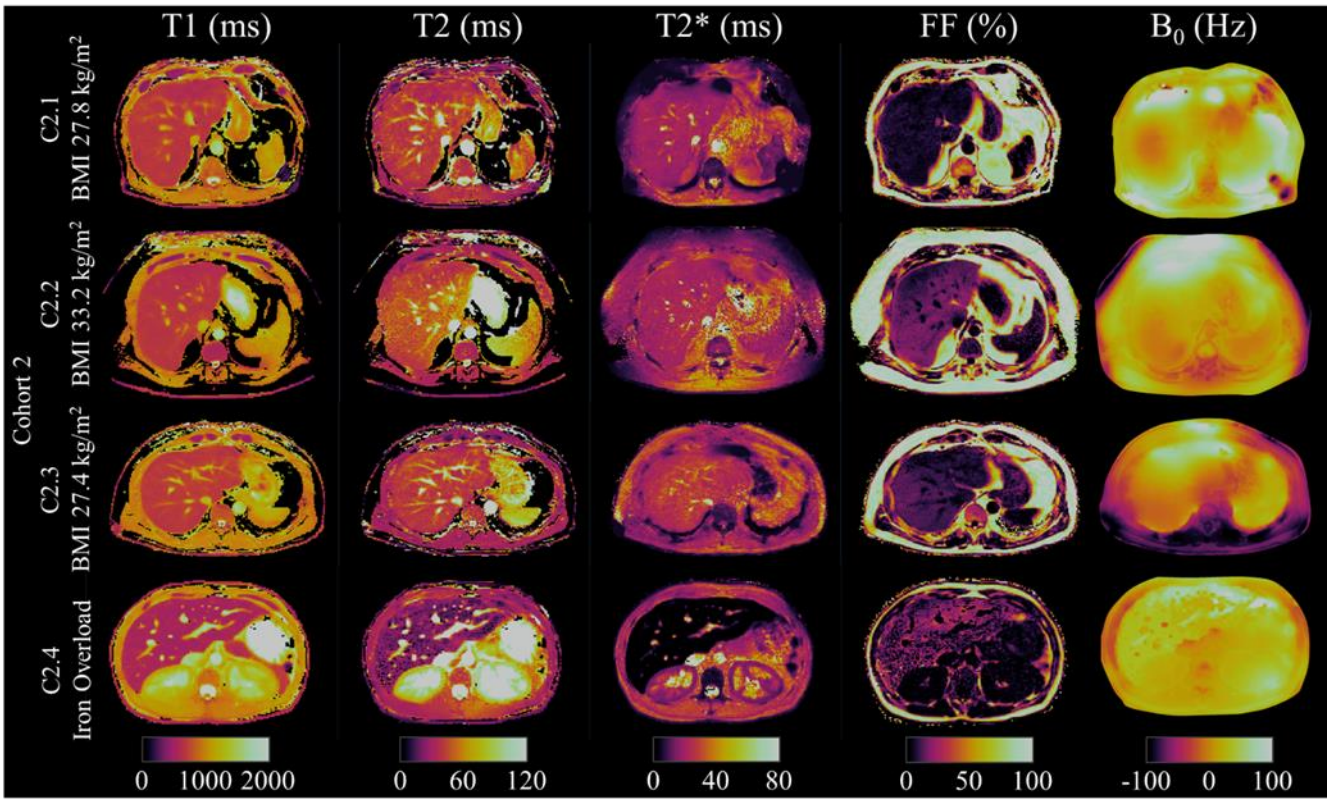

Figure 5. Proposed 9-echo liver MRF water T_1, water T_2, T_2*, FF and B_0 maps acquired in a single breath-hold in three patients with large BMI and one with iron overload. An elevated hepatic fat content of 15.25%, 12.45% and 18% was measured for subjects C2.2, C2.3 and C2.4 respectively. Subject C2.4 presented abnormally low water T_1, water T_2 and T_2* consistent with previously diagnosed elevated hepatic iron content.

Supporting Information Captions

Supporting Information Text S1: Number of echoes required for liver MRF T_2* estimation

Supporting Information Text S2: Liver MRF simulations

A) Fat model parameters

	T1	T2	ppm	Peak weight
Water	Dictionary	Dictionary	0	N/A
Fat peak 1	543	80	3.8	0.087
Fat peak 2	260	55	3.4	0.693
Fat peak 3	225	52	2.6	0.128
Fat peak 4	284	46	1.94	0.004
Fat peak 5	154	50	0.39	0.039
Fat peak 6	420	44	-0.6	0.048

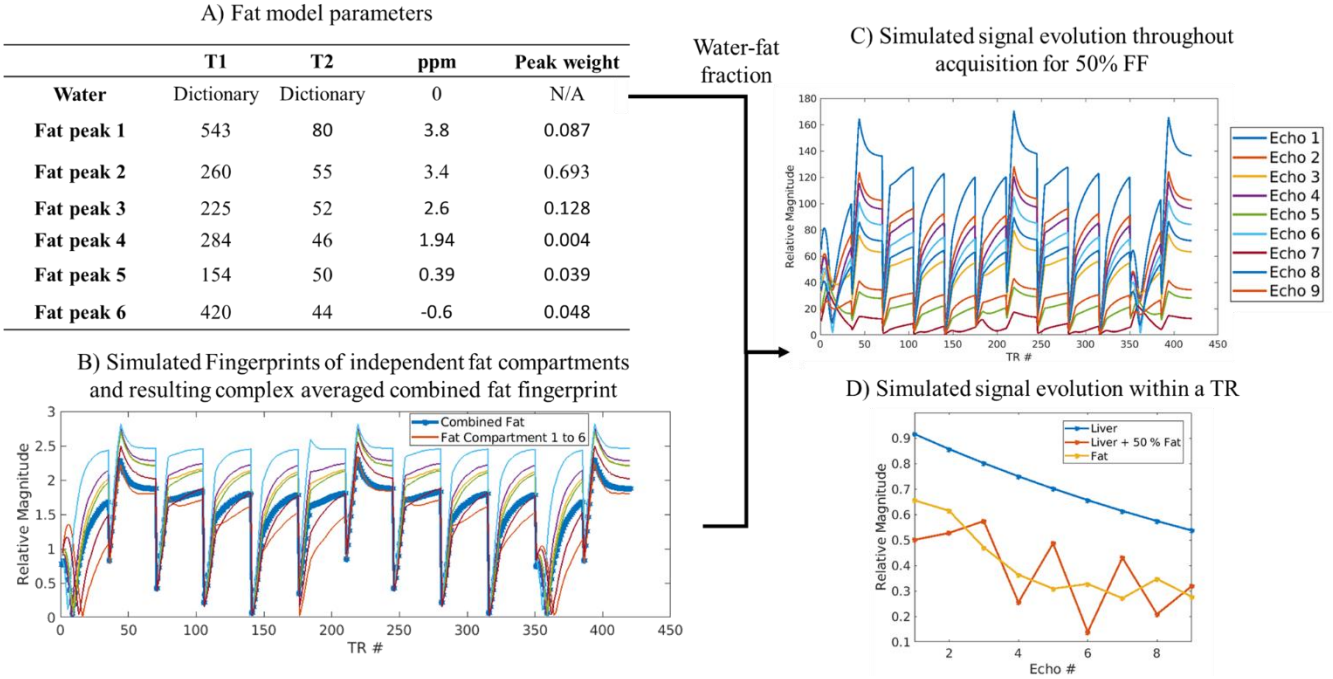

Supporting Information Figure S1. A) T_1, T_2, chemical shift (ppm) and peak weight for each of the 6 peaks considered for fat. B) The six peak and combined fat signal evolutions are simulated using the EPG framework and model parameters provided in (A). C) Example of a simulated signal evolution for a 50-50% mix of liver (water T_1= 650ms, water T_2= 50ms) and fat. D) Within TR signal evolution for pure liver, pure fat and 50-50% mix for the first MRF timepoint.

	IRSE	MESE	12 echo GRE	MOLLI 5(3)3	T2-GRASE
FOV(mm^2)	192x192	192x192	352x352	352x352	352x352
Resolution (mm^2)	2x2	2x2	2x2	2x2	2x2
Slice thickness (mm)	8	8	8	8	8
Readout	Cartesian	Cartesian	Cartesian (fly-back, 4 Averages)	Cartesian	EPI (EPI factor 9)
Flip angle (°)	90	90	5	50	90
TR/TE(/ΔTE) (ms)	7000/shortest	7000/15/15 (8 echoes)	27/1.5/2 (12 echoes)	2.61/1.32	1000/8.3/8.3 (9 echoes)
TI1/TImax (ms)	50/3000 (9 inversion times)	x	x	82/300	x
Bandwidth (Hz/pixel)	120	92	1085	1153	1430 (frequency direction)
SENSE factor	Fully sampled	Fully sampled	2	2	2
Scan time	~1h40min	11min	11s	11s	15s
Model	$A(1-Be^{-t/T1})$	$M_0\ e^{-t/T2}$	Six peak fat model and single T2* decay	$A(1-Be^{-t/T1^*})$	$M_0\ e^{-t/T2}$
Fitting algorithm	Levenberg-Marquardt	Levenberg-Marquardt	Graphcut	Scanner (Maximum Likelihood)	Scanner (Maximum Likelihood)

Supporting Information Table S1. Acquisition and reconstruction parameters for reference phantom mapping sequences (IRSE, MESE and 12-echo GRE) and conventional in vivo sequences (MOLLI, T2-GRASE, 12-echo GRE).

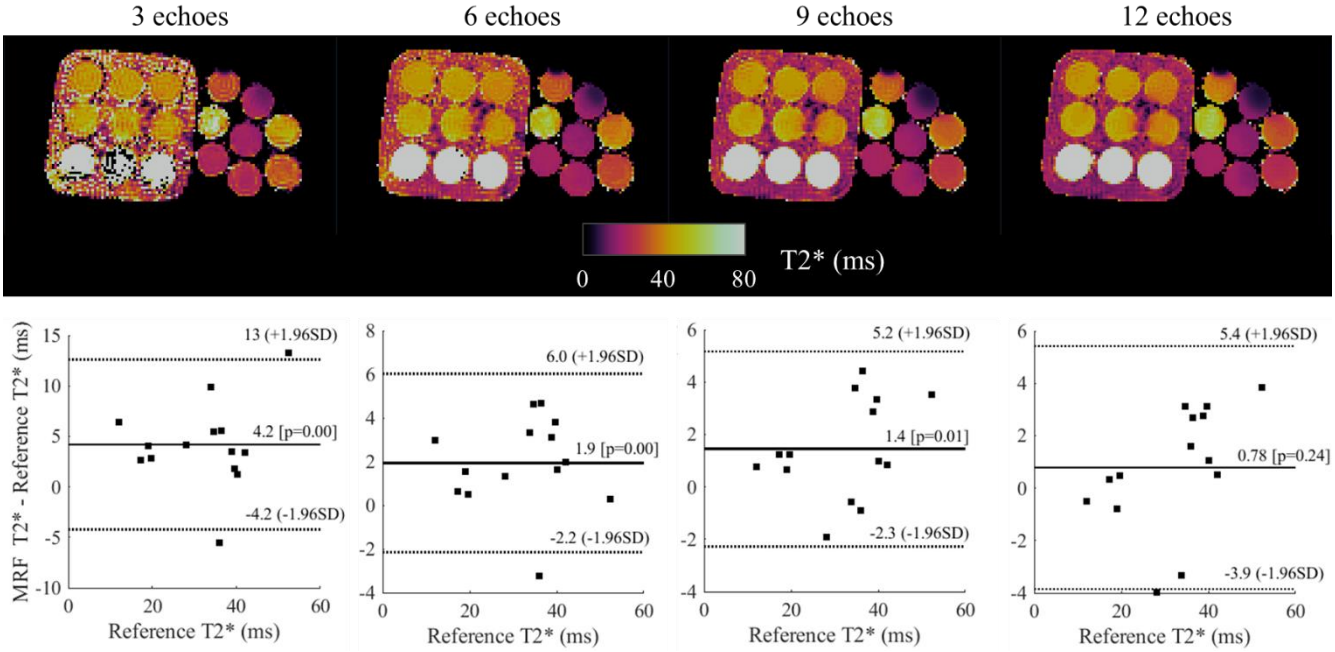

Supporting Information Figure S2. A) T_2* maps obtained using the proposed MRF framework and the first 3, 6, 9 and 12 echoes of a 12-echo MRF acquisition. B) Corresponding Bland-Altmann plots comparing 3, 6, 9 and 12 echoes MRF T_2* measurements with the

reference measurement (12-echo GRE). Please note that the vertical scales change between the plots.

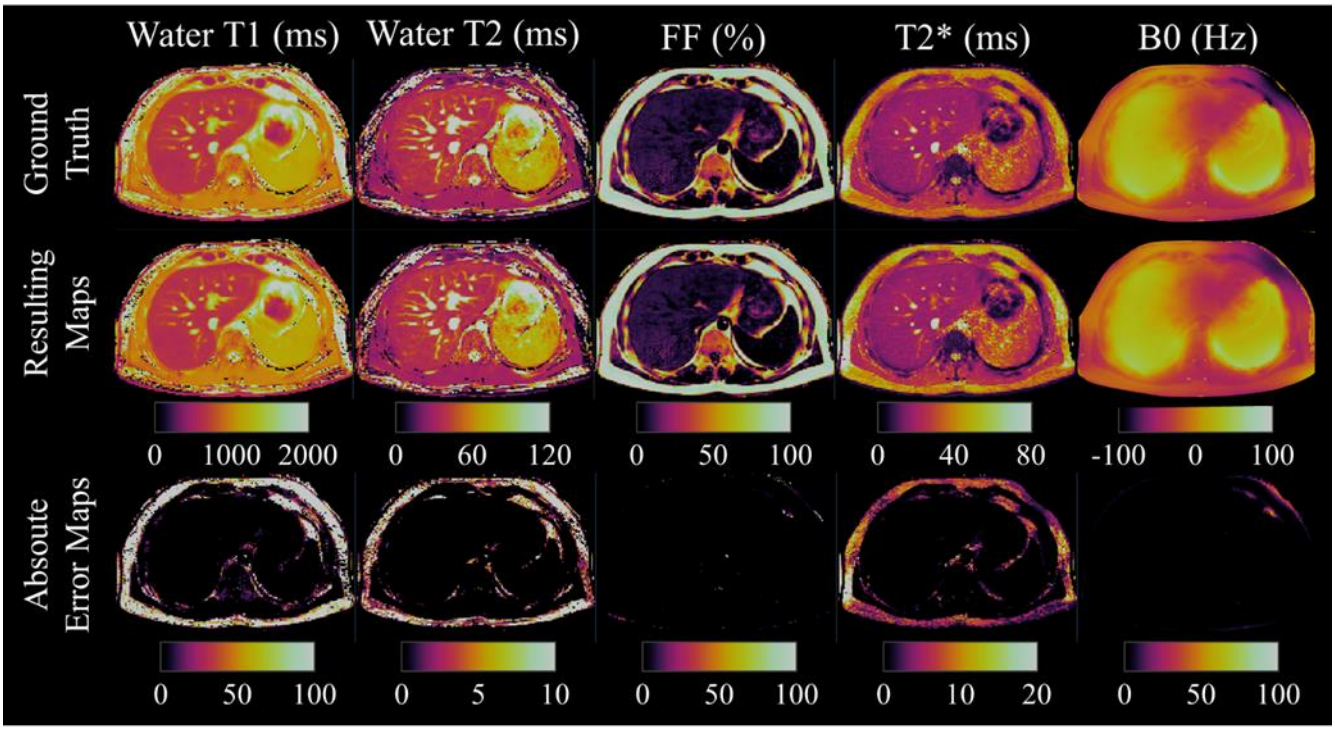

Supporting Information Figure S3. Numerical simulations from realistic water T_1, water T_2, FF, T_2* and B_0 maps (Ground Truth, top row) and resulting maps obtained using the proposed framework (second row). Absolute error in the liver was <1% for all parameters (third row). T_2* estimation errors in the subcutaneous fat in simulations suggests that the fixed peak weight model induces T_2* overestimation in fat. T_2* overestimation in fat was also observed in vivo experiments.

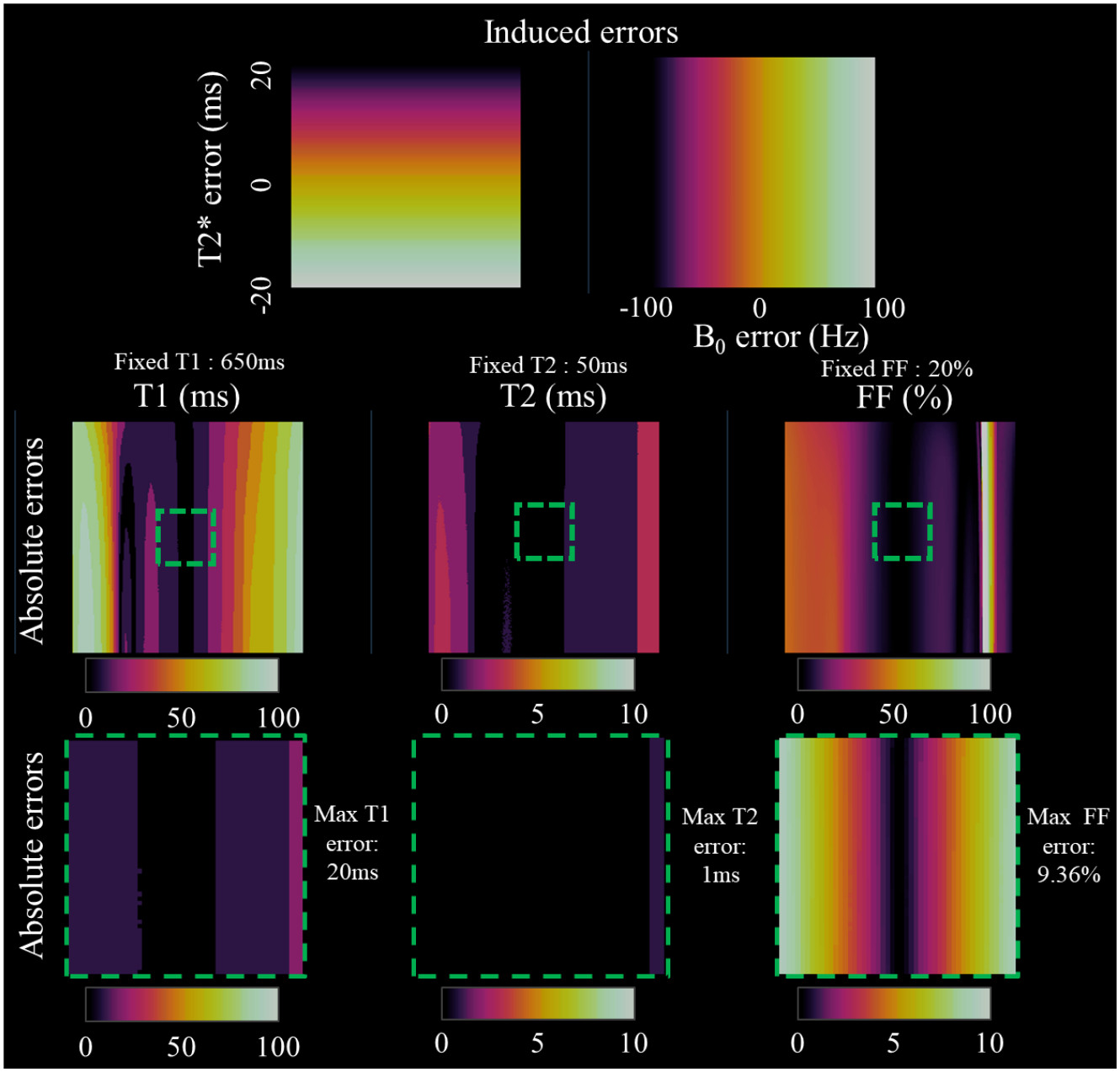

Supporting Information Figure S4. Numerical simulations with fixed water T_1 (650 ms), water T_2 (50 ms), FF (20 %), B_0 (0 Hz) and T_2* (30 ms). Errors were introduced to the B_0 field (left-right gradient) and T_2* (top-down gradient) estimations (Top row) and used instead of the estimated maps before water-fat separation. The resulting absolute errors for water T_1, water T_2 and FF estimation (second row) and zoom in ([-4:4] for T_2* errors and [-20:20 Hz] errors) on the absolute error maps (third row) are shown. The third row exhibited maximum errors of 20ms, 1ms and 9.36% errors for water T_1, water T_2 and FF estimation respectively.

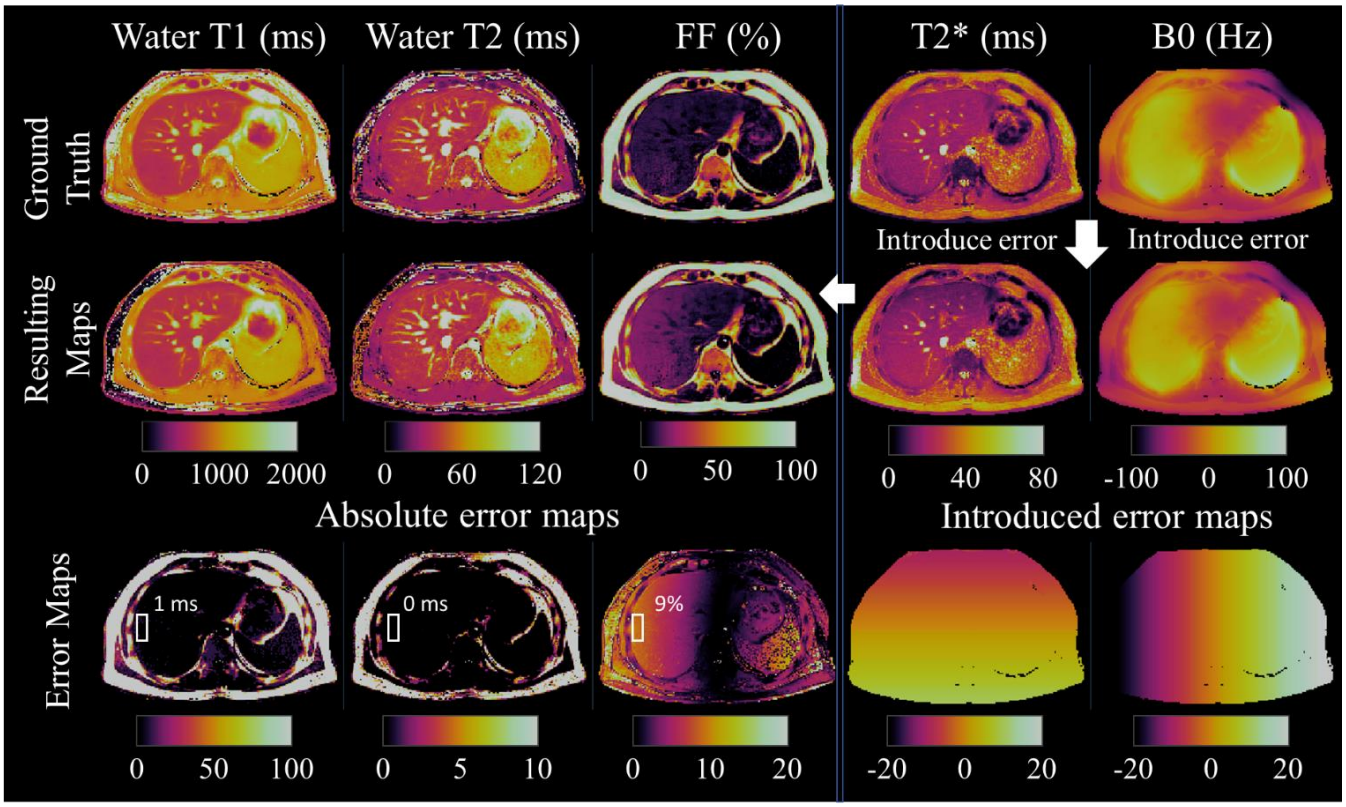

Supporting Information Figure S5. Numerical simulations from realistic water T_1, water T_2 and FF maps. Errors were introduced to the B_0 field (left-right gradient) and T_2* (top-down gradient) estimations and used instead of the normally estimated maps before water-fat separation to generate the resulting water T_1, water T_2 and FF maps (second row) with the proposed MRF approach. Corresponding absolute error maps and reported liver error (white ROI) are shown in the third row.

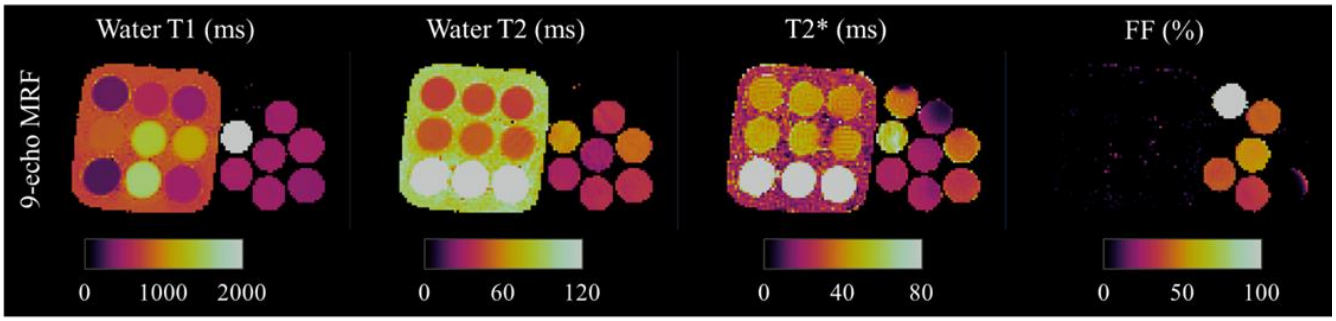

Supporting Information Figure S6. Proposed 9-echo MRF phantom T_1, T_2, T_2* and FF maps acquired in a 13.9s scan.

11 Subjects		Liver			Muscle			Spleen			Subcutaneous fat		
		MRF (water)	Conv.	Literature	MRF (water)	Conv.	Literature	MRF (water)	Conv.	Literature	MRF (fat)	Conv.	Literature
T1 (ms)	Average	676	585	570-586	1000	844	856-891	1235	1150	1026-1057	270	266	200-343
	Range	[607, 803]	[491, 758]		[955, 1029]	[774, 901]		[1130,1287]	[1042,1209]		[261, 281]	[86, 537]	
T2 (ms)	Average	43.6	50.5	35-46	30.7	39.0	27-60	91.0	104.3	~79	97.0	126.3	52-58
	Range	[35.9, 57.8]	[42.0, 68.0]		[28.7, 34.5]	[35.2, 47.7]		[68.8, 104]	[81.3,122.6]		[90.6,110.8]	[101, 143.5]	

11 Subjects		Liver			Muscle			Spleen			Subcutaneous fat		
		MRF	Conv.	Literature	MRF	Conv.	Literature	MRF	Conv.	Literature	MRF	Conv.	Literature
T2* (ms)	Average	30.1	31.5	~28.1	24.9	26.0	N/A	69.5	64.9	~43.9	34.0	27.0	N/A
	Range	[17.9, 39]	[22.2, 41.5]		[13.3, 29.5]	[11, 31]		[31.8, 99.1]	[34.9, 86.8]		[14, 44.7]	[11.7, 34.5]	
FF (%)	Average	2.56	2.0	~2.11	1.6	2.3	N/A	0.7	0.6	N/A	87.2	86.0	N/A
	Range	[1.2, 5.3]	[1.2, 5.3]		[-1.6, 2.8]	[0.7, 7.9]		[-4.3, 2.3]	[-0.1, 2.7]		[70.3, 93.4]	[71.9, 94.4]	

Supporting Information Table S2. Reported average and range of values ([min, max]) observed in 11 subjects (C1.1-11) with no history of liver disease using the proposed 9-echo liver MRF and conventional MOLLI, T_2-GRASE and 12-echo GRE (T_2*/FF) for the liver, muscle, spleen and subcutaneous fat. Literature values when available were reported for T_1 (34), T_2 (34), T_2* (35) and FF (36). Please note that MRF water T_1 and MRF water T_2 values are reported for the liver, muscle and spleen and MRF fat T_1 and MRF fat T_2 values for subcutaneous fat.

References

1. Younossi Z, Tacke F, Arrese M, et al. Global Perspectives on Nonalcoholic Fatty Liver Disease and Nonalcoholic Steatohepatitis. Hepatology 2019;69:2672–2682 doi: 10.1002/hep.30251.
2. Dowman JK, Tomlinson JW, Newsome PN. Systematic review: the diagnosis and staging of non-alcoholic fatty liver disease and non-alcoholic steatohepatitis. Alimentary pharmacology & therapeutics 2011;33:525–40 doi: 10.1111/j.1365-2036.2010.04556.x.
3. Kleiner DE, Brunt EM, Van Natta M, et al. Design and validation of a histological scoring system for nonalcoholic fatty liver disease. Hepatology 2005;41:1313–1321 doi: 10.1002/hep.20701.
4. Meisamy S, Hines CDG, Hamilton G, et al. Quantification of Hepatic Steatosis with T1-independent, T2*-corrected MR Imaging with Spectral Modeling of Fat: Blinded Comparison with MR Spectroscopy. Radiology 2011;258:767–775 doi: 10.1148/radiol.10100708.
5. Reeder SB, Sirlin CB. Quantification of liver fat with magnetic resonance imaging. Magnetic resonance imaging clinics of North America 2010;18 (3):337–57 doi: 10.1016/j.mric.2010.08.013.
6. Wood JC, Enriquez C, Ghugre N, et al. MRI R2 and R2* mapping accurately estimates hepatic iron concentration in transfusion-dependent thalassemia and sickle cell disease patients. Blood 2005;106:1460–1465 doi: 10.1182/blood-2004-10-3982.
7. Thomsen C, Christoffersen P, Henriksen O, Juhl E. Prolonged T1 in patients with liver cirrhosis: An in vivo MRI study. Magnetic Resonance Imaging 1990;8:599–604 doi: 10.1016/0730-725X(90)90137-Q.
8. Venkatesh SK, Yin M, Ehman RL. Magnetic resonance elastography of liver: Technique, analysis, and clinical applications. Journal of Magnetic Resonance Imaging 2013;37:544–555 doi: 10.1002/jmri.23731.
9. Banerjee R, Pavlides M, Tunnicliffe EM, et al. Multiparametric magnetic resonance for the non-invasive diagnosis of liver disease. Journal of Hepatology 2014;60:69–77 doi: 10.1016/J.JHEP.2013.09.002.
10. Pavlides M, Banerjee R, Sellwood J, et al. Multiparametric magnetic resonance imaging predicts clinical outcomes in patients with chronic liver disease. Journal of Hepatology 2016;64:308–315 doi: 10.1016/J.JHEP.2015.10.009.
11. Yu H, McKenzie CA, Shimakawa A, et al. Multiecho reconstruction for simultaneous water-fat decomposition and T2* estimation. Journal of Magnetic Resonance Imaging

2007;26:1153–1161 doi: 10.1002/jmri.21090.
12. Chen Y, Jiang Y, Pahwa S, et al. MR Fingerprinting for Rapid Quantitative Abdominal Imaging. Radiology 2016;279:278–286 doi: 10.1148/radiol.2016152037.
13. Reeder SB, Pineda AR, Wen Z, et al. Iterative decomposition of water and fat with echo asymmetry and least-squares estimation (IDEAL): Application with fast spin-echo imaging. Magnetic Resonance in Medicine 2005;54:636–644 doi: 10.1002/mrm.20624.
14. Yu H, Shimakawa A, McKenzie CA, Brodsky E, Brittain JH, Reeder SB. Multiecho water-fat separation and simultaneous R2* estimation with multifrequency fat spectrum modeling. Magnetic Resonance in Medicine 2008;60:1122–1134 doi: 10.1002/mrm.21737.
15. Ma D, Gulani V, Seiberlich N, et al. Magnetic resonance fingerprinting. Nature 2013;495:187–92 doi: 10.1038/nature11971.
16. Ostenson J, Damon BM, Welch EB. MR fingerprinting with simultaneous T1, T2, and fat signal fraction estimation with integrated B0 correction reduces bias in water T1 and T2 estimates. Magnetic Resonance Imaging 2019;60:7–19 doi: 10.1016/J.MRI.2019.03.017.
17. Jaubert O, Cruz G, Bustin A, et al. Water–fat Dixon cardiac magnetic resonance fingerprinting. Magnetic Resonance in Medicine 2020;83:2107–2123 doi: 10.1002/mrm.28070.
18. Hernando D, Kellman P, Haldar JP, Liang Z-P. Robust water/fat separation in the presence of large field inhomogeneities using a graph cut algorithm. Magnetic Resonance in Medicine 2010;63:79–90 doi: 10.1002/mrm.22177.
19. Nezafat R, Stuber M, Ouwerkerk R, Gharib AM, Desai MY, Pettigrew RI. B1-insensitiveT2 preparation for improved coronary magnetic resonance angiography at 3 T. Magnetic Resonance in Medicine 2006;55:858–864 doi: 10.1002/mrm.20835.
20. Hamilton JI, Jiang Y, Ma D, et al. Investigating and reducing the effects of confounding factors for robust T1 and T2 mapping with cardiac MR fingerprinting. Magnetic Resonance Imaging 2018;53:40–51 doi: 10.1016/J.MRI.2018.06.018.
21. Guzek B, Korzdorfer G, Nittka M, Pfeuffer J. Influence of Off-resonance on FISP Magnetic Resonance Fingerprinting (FISP-MRF). Proc. Intl. Soc. Mag. Reson. Med. 26 2018:4264.
22. Jiang Y, Ma D, Seiberlich N, Gulani V, Griswold MA. MR fingerprinting using fast imaging with steady state precession (FISP) with spiral readout. Magnetic Resonance in Medicine 2015;74:1621–1631 doi: 10.1002/mrm.25559.
23. Bustin A, Cruz G, Jaubert O, Karina L, Botnar RM, Prieto C. High-Dimensionality Undersampled Patch-Based Reconstruction (HD-PROST) for Accelerated Multi-Contrast

Magnetic Resonance Imaging. Magnetic Resonance in Medicine 2019;81:3705–3719 doi: 10.1002/mrm.27694.
24. Assländer J, Cloos MA, Knoll F, Sodickson DK, Hennig J, Lattanzi R. Low rank alternating direction method of multipliers reconstruction for MR fingerprinting. Magnetic Resonance in Medicine 2018;79:83–96 doi: 10.1002/mrm.26639.
25. McGivney DF, Pierre E, Ma D, et al. SVD Compression for Magnetic Resonance Fingerprinting in the Time Domain. IEEE Transactions on Medical Imaging 2014;33:2311–2322 doi: 10.1109/TMI.2014.2337321.
26. Dixon WT. Simple proton spectroscopic imaging. Radiology 1984;153:189–194 doi: 10.1148/radiology.153.1.6089263.
27. Yeung HN, Kormos DW. Separation of true fat and water images by correcting magnetic field inhomogeneity in situ. Radiology 1986;159:783–786 doi: 10.1148/radiology.159.3.3704157.
28. Hamilton G, Smith DL, Bydder M, Nayak KS, Hu HH. MR properties of brown and white adipose tissues. Journal of Magnetic Resonance Imaging 2011;34:468–473 doi: 10.1002/jmri.22623.
29. Hernando D, Haldar JP, Sutton BP, Ma J, Kellman P, Liang Z-P. Joint estimation of water/fat images and field inhomogeneity map. Magnetic Resonance in Medicine 2008;59:571–580 doi: 10.1002/mrm.21522.
30. Weigel M. Extended phase graphs: Dephasing, RF pulses, and echoes - Pure and simple. Journal of Magnetic Resonance Imaging 2015;41:266–295 doi: 10.1002/jmri.24619.
31. Ma D, Coppo S, Chen Y, et al. Slice profile and B_1 corrections in 2D magnetic resonance fingerprinting. Magnetic Resonance in Medicine 2017;78:1781–1789 doi: 10.1002/mrm.26580.
32. Captur G, Gatehouse P, Kellman P, et al. A T1 and ECV phantom for global T1 mapping quality assurance: The T1 mapping and ECV standardisation in CMR (T1MES) program. Journal of Cardiovascular Magnetic Resonance 2016;18:W14 doi: 10.1186/1532-429X-18-S1-W14.
33. Liu C-Y, McKenzie CA, Yu H, Brittain JH, Reeder SB. Fat quantification with IDEAL gradient echo imaging: Correction of bias from T1 and noise. Magnetic Resonance in Medicine 2007;58:354–364 doi: 10.1002/mrm.21301.
34. De Bazelaire CMJ, Duhamel GD, Rofsky NM, Alsop DC. MR Imaging Relaxation Times of Abdominal and Pelvic Tissues Measured in Vivo at 3.0 T: Preliminary Results. Radiology 2004;230:652–659 doi: 10.1148/radiol.2303021331.

35. Schwenzer NF, Machann J, Haap MM, et al. T2* Relaxometry in Liver, Pancreas, and Spleen in a Healthy Cohort of One Hundred Twenty-Nine Subjects–Correlation With Age, Gender, and Serum Ferritin. Investigative Radiology 2008;43:854–860 doi: 10.1097/RLI.0b013e3181862413.
36. Wilman HR, Kelly M, Garratt S, et al. Characterisation of liver fat in the UK Biobank cohort Lu S-N, editor. PLOS ONE 2017;12:e0172921 doi: 10.1371/journal.pone.0172921.
37. Marty B, Carlier PG. MR fingerprinting for water T1 and fat fraction quantification in fat infiltrated skeletal muscles. Magnetic Resonance in Medicine 2020;83:621–634 doi: 10.1002/mrm.27960.
38. Cencini M, Biagi L, Kaggie JD, Schulte RF, Tosetti M, Buonincontri G. Magnetic resonance fingerprinting with dictionary-based fat and water separation (DBFW MRF): A multi-component approach. Magnetic Resonance in Medicine 2019;81(5):3032–3045 doi: 10.1002/mrm.27628.
39. Berglund J, Johansson L, Ahlström H, Kullberg J. Three-point dixon method enables whole-body water and fat imaging of obese subjects. Magnetic Resonance in Medicine 2010;63:1659–1668 doi: 10.1002/mrm.22385.
40. Koolstra K, Webb AG, Veeger TTJ, Kan HE, Koken P, Börnert P. Water–fat separation in spiral magnetic resonance fingerprinting for high temporal resolution tissue relaxation time quantification in muscle. Magnetic Resonance in Medicine 2020:mrm.28143 doi: 10.1002/mrm.28143.
41. Nolte T, Gross-Weege N, Doneva M, et al. Spiral blurring correction with water–fat separation for magnetic resonance fingerprinting in the breast. Magnetic Resonance in Medicine 2020;83:1192–1207 doi: 10.1002/mrm.27994.
42. Hilbert T, Xia D, Block KT, et al. Magnetization transfer in magnetic resonance fingerprinting. Magnetic Resonance in Medicine 2019:mrm.28096 doi: 10.1002/mrm.28096.
43. Flassbeck S, Schmidt S, Bachert P, Ladd ME, Schmitter S. Flow MR fingerprinting. Magnetic Resonance in Medicine 2019;81:2536–2550 doi: 10.1002/mrm.27588.
44. Malik SJ, Teixeira RPAG, Hajnal J V. Extended phase graph formalism for systems with magnetization transfer and exchange. Magnetic Resonance in Medicine 2018;80:767–779 doi: 10.1002/mrm.27040.
45. Robson MD, Piechnik SK, Tunnicliffe EM, Neubauer S. T1 measurements in the human myocardium: The effects of magnetization transfer on the SASHA and MOLLI sequences. Magnetic Resonance in Medicine 2013;70:664–670 doi: 10.1002/mrm.24867.
46. Roujol S, Weingärtner S, Foppa M, et al. Accuracy, Precision, and Reproducibility of

Four T1 Mapping Sequences: A Head-to-Head Comparison of MOLLI, ShMOLLI, SASHA, and SAPPHIRE. Radiology 2014;272:683–689 doi: 10.1148/radiol.14140296.
47. Tirkes T, Zhao X, Lin C, et al. Evaluation of variable flip angle, MOLLI, SASHA, and IR-SNAPSHOT pulse sequences for T1 relaxometry and extracellular volume imaging of the pancreas and liver. Magnetic Resonance Materials in Physics, Biology and Medicine 2019;32:559–566 doi: 10.1007/s10334-019-00762-2.
48. Baeßler B, Schaarschmidt F, Stehning C, Schnackenburg B, Maintz D, Bunck AC. A systematic evaluation of three different cardiac T2-mapping sequences at 1.5 and 3T in healthy volunteers. European Journal of Radiology 2015;84:2161–2170 doi: 10.1016/J.EJRAD.2015.08.002.
49. Hamilton JI, Jiang Y, Chen Y, et al. MR fingerprinting for rapid quantification of myocardial T1, T2, and proton spin density. Magnetic Resonance in Medicine 2017;77:1446–1458 doi: 10.1002/mrm.26216.
50. Bachtiar V, Kelly MD, Wilman HR, et al. Repeatability and reproducibility of multiparametric magnetic resonance imaging of the liver. PLOS ONE 2019;14:e0214921 doi: 10.1371/journal.pone.0214921.
51. Le T-A, Chen J, Changchien C, et al. Effect of colesevelam on liver fat quantified by magnetic resonance in nonalcoholic steatohepatitis: A randomized controlled trial. Hepatology 2012;56:922–932 doi: 10.1002/hep.25731.
52. Middleton MS, Heba ER, Hooker CA, et al. Agreement Between Magnetic Resonance Imaging Proton Density Fat Fraction Measurements and Pathologist-Assigned Steatosis Grades of Liver Biopsies From Adults With Nonalcoholic Steatohepatitis. Gastroenterology 2017;153:753–761 doi: 10.1053/j.gastro.2017.06.005.
53. Loomba R, Sirlin CB, Ang B, et al. Ezetimibe for the treatment of nonalcoholic steatohepatitis: Assessment by novel magnetic resonance imaging and magnetic resonance elastography in a randomized trial (MOZART trial). Hepatology 2015;61:1239–1250 doi: 10.1002/hep.27647.
54. Tunnicliffe EM, Banerjee R, Pavlides M, Neubauer S, Robson MD. A model for hepatic fibrosis: the competing effects of cell loss and iron on shortened modified Look-Locker inversion recovery T_1 (shMOLLI- T_1) in the liver. Journal of Magnetic Resonance Imaging 2017;45:450–462 doi: 10.1002/jmri.25392.